Optical and structural properties of GaSb-doped Mn based diluted magnetic semiconductor thin films grown via DC magnetron sputtering

Jorge A. Calderón, Heiddy P. Quiroz, A. Dussan*

Department of Physics, Group of Nanostructured Materials and their Applications, Universidad Nacional de Colombia – Bogotá and Street address: Cra. 30 No. 45-03 Edificio 404 Lab. 121C Ciudad Universitaria, 11001, Colombia

*Corresponding author. Tel: (+57) 1-3165000; E-mail: adussanc@unal.edu.co

Received: 15 September 2016, Revised: 27 October 2016 and Accepted: 20 November 2016

DOI: 10.5185/amlett.2017.7110
www.vbripress.com/aml

Abstract

In this work, diluted magnetic semiconductor GaSb:Mn thin films were grown via DC magnetron Co-sputtering on glass substrates. The effect of synthesis parameters on the optical and structural properties was determined through spectral transmittance measurements and X-ray diffraction (XRD), respectively. Substrate temperature was changed from 373 to 523 K and layer thicknesses were obtained between 200 and 330 nm. All samples were subjected to annealing process to 623 K in situ. It was found that the optical constants (refractive index (n), absorption coefficient (α), extinction coefficient (κ), and energy gap (E_1)) are significantly affected by the temperature and target power used during the synthesis process. In particular, a variation of the energy gap between 0.58 and 0.98 eV was obtained when the target power of GaSb varied between 80 and 140 W. GaSb, Mn_2Sb and SiO_2 phases were observed for lowest values of target power, where SiO_2 phase is a contribution of the substrate. The dielectric function of the compound with a dependence on synthesis parameters such as, the substrate temperature and deposition time was obtained, both real (ε_1) and imaginary part (ε_2). Analysis of the XRD measurements allowed to find that the (GaSb)Mn films grow with a mixture of the GaSb and Mn_2Sb phases, and an amorphous halo associated with the glass substrate. A correlation between synthesis parameters and optical properties is presented. Diluted magnetic semiconductors, like GaSb:Mn, are considered among promising materials for the development of new spin-electronic devices, high speed quantum-mechanical in computational information, other more; in this case, studies on magnetic properties in digital alloys of GaSb/Mn can be realized around of the optimization of Curie temperature.

Keywords: Diluted semiconductor, GaMnSb, sputtering method, spintronics.

Introduction

Diluted magnetic semiconductors (DMS) are studied for a vast number of applications in spintronic devices due to the influence of their magnetic, optical, electrical, and transport properties. Within this important group of semiconductor materials, II-VI / III-V doped with Mn, we can find GaMnAs [**1**], ZnMnO [**2**], InMnAs [**3**], and GaSb:Mn [**4**]. In the last case, the GaSb:Mn has been studied because the GaSb semiconductor matrix is an important compound for research in quantum dots [**5**], thin films for radiation detection devices [**6**], solar cells [**7,8**], and optical communication technology devices [**9**], among others. The biggest obstacle to obtaining a manufacturing process based on GaMnSb devices is their low Curie temperature (~25 K); however, recent studies show the possibility of obtaining the ternary compound with Curie temperatures above 30 K [**10**]. The experimental and theoretical states of DMS fabrication are very complex due to difficulties in the synthesis of this material related to low concentrations of the magnetic elements (between 5 - 10%) on the semiconductor matrix [**11-13**] and differences in theoretical prediction of high-temperature ferromagnetic characteristic, and other properties [**13-15**].

Although much interest exists in studying DMS materials with high critical temperature (T_C), the ferromagnetic nature of the compound and its influence with annealing temperature is not yet clear, given the condition of the DMS as a non-equilibrium state system. This material is studied for applications in systems, such as spin injectors [**16**], a wide range of magnetic field sensors [**17**], optical read-write memories based on optical alignment of bound magnetic polarons [**17,18**], among others.

This work presents a study of optical and structural properties of GaSb:Mn thin films deposited via DC magnetron co-sputtering, changing the magnetron power of the GaSb target and substrate temperature. From the Swanepoel method and Beer's law, optical properties were calculated, including: refractive index (n), extinction coefficient (κ), and energy gap (E_g), and real part (ε_1) - imaginary part (ε_2) of the dielectric function. A correlation between physical properties and synthesis parameters is presented.

Experimental

Synthesis of GaSb:Mn samples

The GaSb:Mn thin films were deposited on glass soda lime type substrates via DC magnetron co-sputtering using a two-magnetron system. GaSb ((Ga) 36.5 (Sb) 63.5 wt%) and Mn targets were used with purities of 99.99% and 99.9%, respectively. The working pressure in the chamber was 2.5×10^{-2}Torr and magnetron power was changed from 80 to 140 W for the GaSb target and 65 W for the Mn target. Samples were deposited in Ar (99.999%) atmosphere at 20 sccm and the substrate temperature (T_s) was varied from 373 to 523 K.

The samples were fabricated by different series. Series 1 consisted of varying magnetron power for the GaSb target from 80 to 140 W, with T_s = 423 K, and maintaining other synthesis parameters constant (substrate temperature, pressure in the chamber, deposition time). In series 2, the deposition process was carried out with T_s at different values: 373, 423, 473, and 523 K, with 100 W magnetron power for the GaSb target and maintaining other synthesis parameters constant. Deposition time and annealing process *in situ* were 15 min and 623 K for both series.

Characterizations

The samples were characterized through XRD measurements by using a Philips X'Pert Pro diffractometer PANalytical equipped with a Cu-Kα source: 1.540598 Å, 40 kV, 40 mA, and an X´Celerator detector. The XRD measurements were performed in the range of $10° \leq 2\theta \leq 90°$ with angular steps of $0.02°$ XRD. The software used for Rietveld refinement of samples was the X'Pert High-Score Plus.

Absorbance spectra and transmittance measurements were obtained using a Cary 5000 spectrophotometer UV-Vis-NIR high yield in the range of 175 to 3300 nm. The band gap and optical parameters were obtained through deconvolution of absorbance and transmittance spectra.

Results and discussion

The transmittance and absorbance spectra for the variation of the GaSb target magnetron power and XRD pattern obtained for the sample with synthesis parameters of 100 W and 423 K substrate temperature were obtained from transmittance and x ray diffraction measurements, respectively (**Fig. 1(a), (b)**). XRD pattern of samples with variation of the GaSb target magnetron power were obtained too (**Fig. 1(c)**). From transmittance spectra (**Fig. 1a)** it is possible to observe that the samples obtained with power values from 100 to 140 W present interference fringes, in contrast with the transmittance spectrum for the sample with 80 W. The local maximum and minimum of the spectra are associated to the interference condition due to the homogeneity of all the samples. The values of n and film thickness for the samples were obtained through the Swanepoel method [**19**].

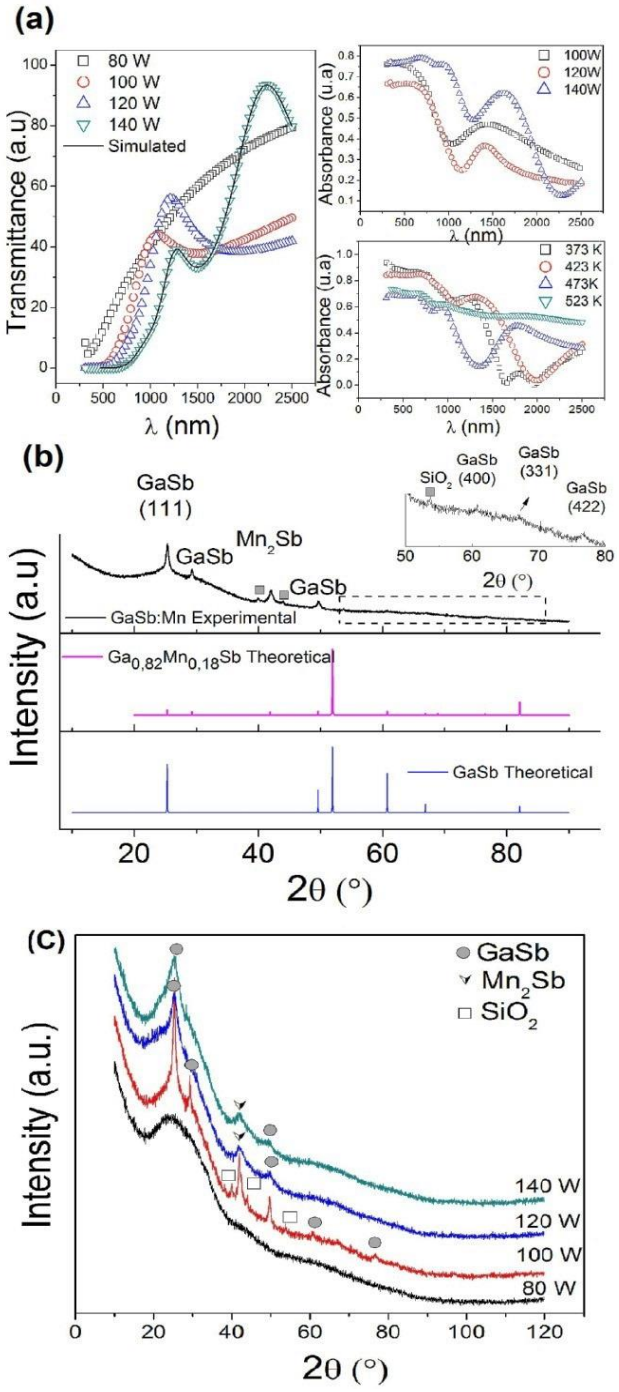

Fig. 1. (a) Transmittance spectra and absorbance measurements of GaSb:Mn, **(b)** XRD pattern of the sample with 100 W and 423 K substrate temperature, **(c)** XRD pattern of the samples varying the power of the GaSb target (T_s = 423 K).

The insets show the absorbance measurements for the samples with power variation from 100 W to 140 W,

together with the absorbance measurements for the samples with T_s variation (**Fig. 1a)**. These Figures shows that the absorbance increases in the ultraviolet and visible region, whilst in the infrared region the absorbance decreased; it is possible to associate to the typical behavior of the GaSb as semiconductor matrix.

The crystalline phases found in the sample with synthesis parameters 100 W and T_s = 423 K are shown in the upper part (**Fig. 1b**). The atomic positions for Ga, Mn, and Sb were obtained using a Density Functional Theory simulation. The theoretical pattern of the ternary compound was simulated using the atomic positions and the X'pert HighScore Plus software. Additionally, the pattern in the bottom (**Fig. 1b)** corresponds to PDF 00-007-0215 database of the GaSb phase with zinc blend structure, crystallographic parameters a = b = c = 6.0950Å and space group F-43m.

From XRD experimental pattern (**Fig. 1b)** is not possible the identification of this material like a DMS due to that GaSb and $Ga_{0.82}Mn_{0.18}Sb$ phases have zinc blend-type structure [**20,21**]. It is observed in the matching peaks between the experimental GaSb:Mn, the GaSb PDF, and the $Ga_{0.82}Mn_{0.18}Sb$ theoretical pattern (**Fig. 1b**). However, the experimental pattern and Rietveltd refinement show presence of the Mn_2Sb phase and the amorphous halo associated with the glass substrate.

On the other hand, T_s variation allows the formation of GaSb and Mn_2Sb phases due to thermal agitation exciting the atoms on the surface and permits the bond among elements. In addition, this provides better adherence of the material deposited on the substrate. Moreover, the competition between Mn_2Sb phase and GaSb phase formation is favored by the co-sputtering method of precursor materials.

Reports of this material deposited over different substrates and methods shows a study with substrate temperature, which affect the phase's formation (**Table 1**).

Table 2. Synthesis parameters reported for GaSb:Mn thin films for different methods (PLD - Pulsed laser deposition and MBE - Molecular beam epitaxy).

Method	Substrate	Ts (K)	Reference
PLD	Single crystal Al_2O_3	373 - 623	[**22**]
MBE	GaAs	548	[**23**]
MBE	GaAs	580	[**24**]
MBE	GaAs	523 - 833	[**25**]

The difference between the magnetron power variation (GaSb and Mn targets) plus the annealing process during film growth influences the structural properties in this material (**Fig. 1c**). In these XRD patterns is possible to observe that an increase of the GaSb target power (**Fig. 1(c)** Power 140 W), which generate a major amount of the atoms of GaSb target to substrate, contributes to the formation of samples more thickness without evidence of the SiO_2 phase in the sample.

The refractive index (n) as a function of the wavelength (λ) for (**Fig. 2(a)**) power variation and (**b**) T_s variation (**Fig. 2(b)**) were obtained from transmittance measurements. The behavior of n is affected by the power variation in the GaSb target (**Fig. 2a**), associated to the competition of the binary phases formation (GaSb and Mn_2Sb). Given that the power of the Mn target is constant, the proportion of atoms emitted remains unchanged, whilst the GaSb proportion and deposition rate were increased. Comparing the behavior of n for an applied power of 100 and 140 W, the tendency is similar, although the n value for the sample at 140 W is greater (**Fig. 2a**).

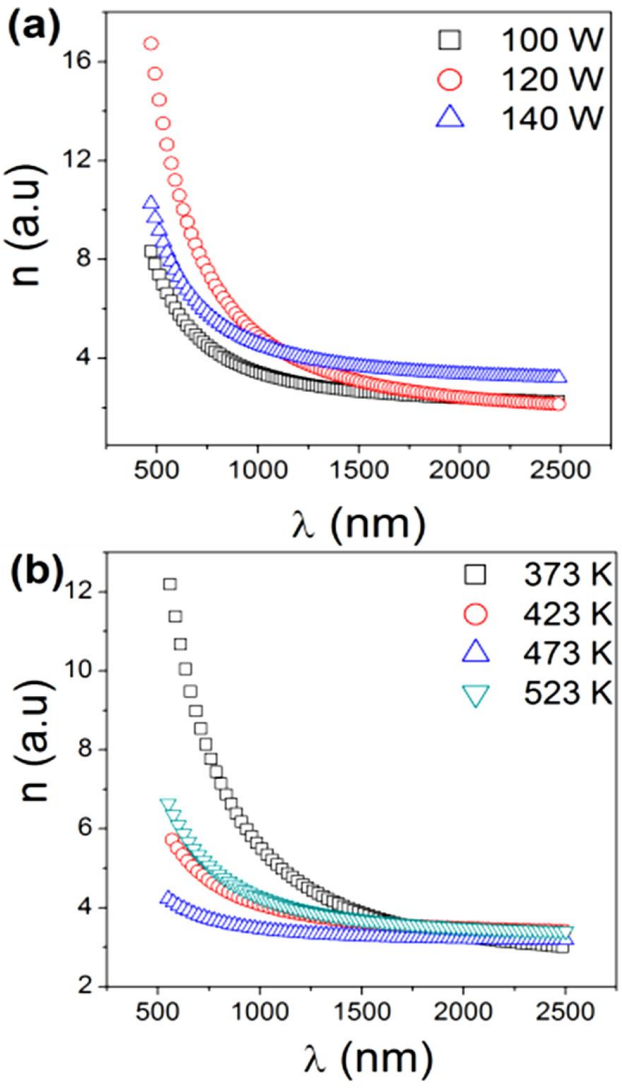

Fig. 2. Refractive index calculated for GaSb:Mn samples varying: **(a)** Magnetron power of the GaSb target, and **(b)** T_s.

Another important optical constant is the extinction coefficient, κ, which is proportional to the probability of absorption of a photon in the sample [**26**]. κ is the probability that an interaction among electrons of the material and the incident electromagnetic wave occurs. κ presents high values around 1900 nm in the case of power variation and around 1500 nm when T_s was 373 and 423 K, respectively (**Fig. 3a)**. The maximum values of κ were between 1900 and 2100 nm when temperatures were 473 and 523 K (**Fig. 3b)**; this is associated to absorption processes. The absorption spectra were obtained as a function of energy (**Fig. 4**) for samples where powers of

the GaSb target and substrate temperature were varied. Absorption coefficient, α, was calculated from the sample thickness and by using Beer's law. The energy gap (E_g) values were obtained from α. In the case of power variation (**Fig. 4a**), the E_g was 0.65 ± 0.01 eV for 120 W; however, by increasing power the gap decreases to 0.58 ± 0.01 eV (**Table 1**). This fact can be associated to the formation of alloys of binary phases (**Fig. 1b**).

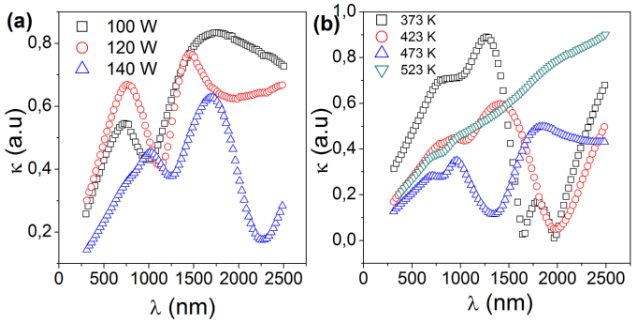

Fig. 3 Extinction coefficient as a function of wavelength, varying: **(a)** Power in GaSb target, and **(b)** T_s.

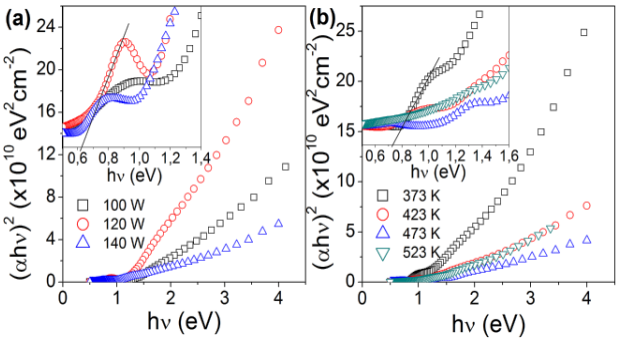

Fig. 4. Absorption curves of the GaSb:Mn samples for both series.

When the substrate temperature was varied (**Fig. 4b**), an increased energy gap was observed from 0.77 ± 0.01 to 0.98 ± 0.01 eV (**Table 2**) in relation to the presence of the GaSb phase, which has an E_g of 0.72 eV [**27**]. This value can vary depending on amorphous fraction and other phases present in the sample [**28,29**]. Hence, the presence of the Mn_2Sb phase strongly affects the energy gap in the samples because it is a metallic alloy [**30, 31**].

Table 2. Energy gap values obtained for the GaSb:Mn samples.

Target Power		Substrate Temperature	
Sample	E_g **(eV) ± 0.01**	**Sample**	E_g **(eV) ± 0.01**
100 W	0.52	373 K	0.77
120 W	0.65	423 K	0.69
140 W	0.58	473 K	0.91
		523 k	0.98

Knowing the extinction coefficient and refractive index, it is possible to determine the real and imaginary parts of the dielectric function, as: $\varepsilon_1 = n^2(\lambda) - \kappa^2(\lambda)$ and $\varepsilon_2 = 2n(\lambda)\kappa(\lambda)$, respectively [**32**].

The real and imaginary parts of the dielectric function for the GaSb:Mn samples as a function of wavelength are shown (**Fig. 5**, **Fig. 6**). In the case of the polar crystal is possible to establish a correlation between ε_1 and the photon incident frequency, when is considered the contribution of free electrons in the valence band of a semiconductor (behavior similar to the metallic). This is according to the observed in the absorbance measurements, where there is an evidence of the high reflectivity (**Fig. 1(a)**).

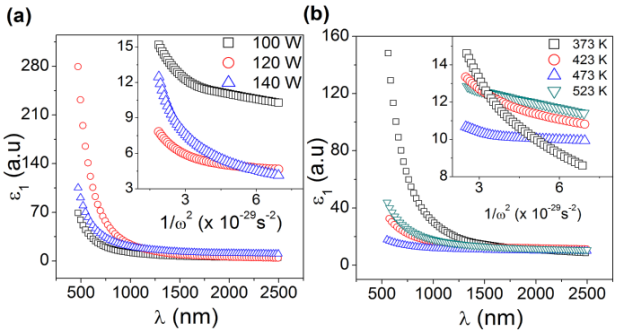

Fig. 5. Real part of the dielectric function of GaSb:Mn samples, varying: **(a)** Power in GaSb target, and **(b)** T_s. Insets in the figures show ε_1 as a function of $1/\varepsilon^2$.

Given that the real part of the dielectric function depends on the plasma frequency (ω_p), it is possible to express ε_1 as:

$$\varepsilon_1 = \varepsilon_\infty - \frac{(\varepsilon_\infty \omega_p^2)}{\omega^2} \qquad (1)$$

Under the conditions $\omega\tau \ll 1$ and $n^2 \gg \kappa^2$ (**Fig. 2**, **Fig. 3**); where τ is the relaxation time, ε_∞ is the limiting value of the high-frequency dielectric function, and ω is the frequency of the incident photon (c/λ) [**32**]. Insets show ε_1 as a function of $1/\omega^2$, where the slope and the intercept are the ω_p and ε_∞, respectively (**Fig. 5(a),(b)**). In the case of power variation in the GaSb target, the ω_p varied between 2.3×10^{14} and 4.4×10^{14} s^{-1}, and ε_∞ between 7.73 and 15.08; this can be associated to the displacement of quasi-free electrons in the valence band as whole, regarding to the positive ions that constitutes the atomic cores. When substrate temperature varies, the values obtained for ω_p and ε_∞ were 3.2×10^{14} s^{-1}, 16.84 for T_s = 373 K, and 2.3×10^{14} s^{-1}, 14.21 for T_s = 523 K. This is possible due to the crystalline phases like GaSb and Mn_2Sb (metallic phase) preponderant in the samples with the increased T_s. This is accompanied by reduced formation of Sb and Mn_2Sb_2 crystals. The variation of ω_p is strongly correlated with the substrate temperature, which agrees with absorbance measurements (Inset **Fig. 1(a)**).

The imaginary part of the dielectric function (ε_2) is non-zero in regions where light is absorbed [**33**]. ε_2 for the samples varying the power of the GaSb target

and substrate temperature, was obtained (**Fig. 6**); it is possible to observe that the range of high absorption is in the infrared region. When T_s was varied, the high absorbance region was located between 1300 and 1900 nm (**Fig. 1**, **Table 2**).

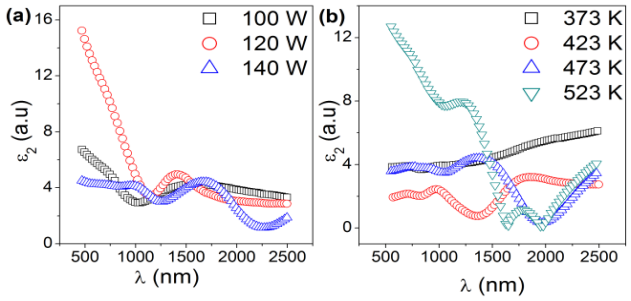

Fig. 6 Imaginary part of the dielectric function of the GaSb:Mn samples, varying: **(a)** Power in the GaSb target, and **(b)** T_s.

Conclusion

GaSb:Mn samples were fabricated via DC magnetron Co-sputtering, varying in a wide range the synthesis parameters. XRD patterns showed the presence of two binary phases GaSb and when the GaSb power and substrate temperature were of 100 W and 623 K, respectively. These phases were identified from Rietveld refinement. It was not possible to establish a single phase of GaSb:Mn compound due to that crystalline planes are the same in comparison with the binary elements; Bragg reflections not represent significant changes about to the positions of the Mn ions. The optical and structural properties of the samples were affected for the variations of the GaSb target power and substrate temperature during the synthesis process. The spectral absorbance measurements showed that GaSb:Mn compound has high absorption regions in the range between 1800 nm and 2100 nm. This absorption can be associated to the presence of the phase, which strongly affects the energy gap in the samples. A correlation between the dielectric function, ε_1, and the plasma frequency, ω_p, was established as a function of synthesis parameters.

Acknowledgements

This work was supported by Universidad Nacional de Colombia - COLCIENCIAS Code: 201010020958.

Author's contributions

All authors contributed equally to the work. Authors have no competing financial interests.

References

1. Riahi, H.; Thevenard, L.; Maaref, M.A.; Gallas, B.; Lemaître, A.; Gourdon, C.; *J. Magn. Magn. Mater.*, **2015**, *395*, 340. **DOI:** 10.1016/j.jmmm.2015.07.090
2. Savchuk, A.I.; Perrone, A.; Lorusso, A.; Stolyarchuk, I.D.; Savchuk, O.A.; Shporta, O.A.; *Appl. Surf. Sci.*, **2014**, *302*, 205. **DOI:** 10.1016/j.apsusc.2013.09.177
3. Peters, J.A.; Wessels, B.W.; *Physica E*, **2010**, *42*, 1447. **DOI:** 10.1016/j.physe.2009.11.107
4. Kamilla, S.K.; Hazra, S.K.; Samantaray, B.K.; Basu, S.; *Solid State Sci.*, **2011**, *13*, 232. **DOI:** 10.1016/j.solidstatesciences.2010.11.020
5. Qiu, F.; Li, Y.; Wang, X.; Zhang, Y.; Zhou, X.; Lv, Y.; Sun, Y.; Deng, H.; Hu, S.; Dai, N.; Wang, C.; Yang, Y.; Zhuang, Q.; Hayne, M.; Krier, A.; *Nanotechnology*, **2016**, *27*, 065602. **DOI:** 10.1088/0957-4484/27/6/065602
6. Vaughan, E.I.; Rahimi, N.; Balakrishnan, G.; Hecht, A. A.; *J. Electron. Mater.*, **2015**, *44*, 3288. **DOI:** 10.1007/s11664-015-3869-3
7. Lee, H.Y.; Huang, H.L.; Pchelyakov, O.P.; Pakhanov, N.A.; *Prog. Photovoltaics Res. Appl.*, **2016**, *24*, 195. **DOI:** 10.1002/pip.2658
8. Yu Wang, Xingwang Zhang, Xiulan Zhang, Nuofu Chen, *Renewable Energy*, **2012**, *48*, 231. **DOI:** 10.1016/j.renene.2012.05.004
9. Jianye, Li.; Wang, Deli.; Ray R. LaPierre (Eds.); Advances in III-V Semiconductor Nanowires and Nanodevices; Bentham eBooks: USA, **2011**. **DOI:** 10.2174/97816080505291110101
10. Zhu, M.Y.; Lu, J.; Ma, J.L.; Li, L.X.; Pan, D.; Zhao, J.H.; *Acta Phys. Sinica*, **2015**, *64*, 077501. **DOI:** 10.7498/aps.64.077501
11. Felser, C.; Fecher, G.H. (eds.); Spintronics from Materials to Devices; Springer: USA, **2013**. **DOI:** 10.1007/978-90-481-3832-6_1
12. Ohno, H.; *Sci.*, **1998**, *281*, 951. **DOI:** 10.1126/science.281.5379.951
13. Dietl, T.; Ohno, H.; Matsukura, F.; Cibert, J.; Ferrand, D.; *Sci.*, **2000**, *287*, 1019. **DOI:** 10.1126/science.287.5455.1019
14. J. Yang, L. Fei, H. Liu, Y. Liu, M. Gao, Y. Zhang, L. Yang *J. Alloy. Compd.*, **2010**, *509*, 3672. **DOI:** 10.1016/j.jallcom.2010.12.157
15. Q. Xu, L. Hartmann, H. Schmidt, H. Hochmuth, M. Lorenz, A. Setzer, P. Esquinazi, C. Meinecke, M. Grundmann, *Thin Solid Films*, **2008**, *516*, 1160. **DOI:** 10.1016/j.tsf.2007.06.145
16. Oh, E.; Lee, B.W.; Kim, T.S.; Lee, J.M.; Oh, S.J.; Song, J.D.; *Curr. Appl. Phys.*, **2012**, *12*, 1244. **DOI:** 10.1016/j.cap.2012.02.041
17. Gaj, J.A.; Kossut, J. (eds.); Introduction to the Physics of Diluted Magnetic Semiconductors; Springer: Berlin, **2010**. **DOI:** 10.1007/978-3-642-15856-8
18. Dietl, T.; Ohno, H.; *Rev. Mod. Phys.*, **2014**, *86*, 187. **DOI:** 10.1103/RevModPhys.86.187
19. Swanepoel, R.; *J. Phps. E: Sci. Instrum.*, **1983**, *16*, 1214. **DOI:** 10.1088/0022-3735/16/12/023
20. Wolska, A.; Klepka, M.T.; Lawniczak-Jablonska, K.; Sadowski, J.; Reszka, A.; Kowalski, B.J.; *Radiat. Phys. Chem.*, **2011**, *80*, 1026. **DOI:** 10.1016/j.radphyschem.2011.02.015
21. Chen, C.; Chen, N.; Liu, L.; Wu, J.; Liu, Z.; Yang, S.; Chai, C.; *J. Cryst. Growth*, **2005**, *279*, 272. **DOI:** 10.1016/j.jcrysgro.2005.02.038
22. A. Talantsev, O. Koplak, R. Morgunov, *Superlattices Microstruct.*, **2016**, *95*, 14. **DOI:** 10.1016/j.spmi.2016.04.012
23. H. Luo, G.B. Kim, M. Cheon, X. Chen, M. Na, S. Wang, B.D. McCombe, X. Liu, Y. Sasaki, T. Wojtowicz, J.K. Furdyna, G. Boishin, L.J. Whitman, *Physica E Low-dimensional Syst. Nanostructures*, **2004**, *20*, 338. **DOI:** 10.1016/j.physe.2003.08.030
24. B.D McCombe, M. Na, X Chen, M Cheon, S. Wang, H Luo, X Liu, Y Sasaki, T Wojtowicz, J.K Furdyna, S.J Potashnik, P Schiffer, *Physica E Low-dimensional Syst. Nanostructures*, **2003**, 16, 90. **DOI:** 10.1016/S1386-9477(02)00594-5
25. F. Matsukura, E. Abe, Y. Ohno, H. Ohno, *Appl. Surf. Sci.*, **2000**, *159-160*, 265. **DOI:** 10.1016/S0169-4332(00)00108-2
26. Albella, J. M. Láminas delgadas y recubrimientos: Preparación, Propiedades y Aplicaciones; Editorial CSIC: España, **2003**, pp. 369-372.
27. Cotirlan, C.; Ghita, R.V.; Negrila, C.C.; Logofatu, C.; Frumosu, F.; Lungu, G.A.; *Appl. Surf. Sci.*, **2016**, *363*, 83. **DOI:** 10.1016/j.apsusc.2015.11.181
28. Kamarudin, M.A.; Hayne1, M.; Zhuang, Q.D.; Kolosov, O.; Nuytten, T.; Moshchalkov, V.V.; Dinelli, F.; J. *Phys. D: Appl. Phys.*, **2010**, *43*, 065402.

DOI: 10.1088/0022-3727/43/6/065402
29. Kunrugsa, M.; Hoo K.; Tung, P.; Danner, A.J.; Panyakeow, S.; Ratanathammaphan, S.; *J. Cryst. Growth*, **2015**, *425*, 287. **DOI:** 10.1016/j.jcrysgro.2015.01.018
30. Kotani, A.; Suzuki, N. (Eds.); Recent Advances in Magnetism of Transition Metal Compounds; World Scientific Publishing: London, **1993**.
31. Motizuki, K.; Ido, H.; Itoh, T.; Morifuji, M. Electronic Structure and Magnetism of 3d-Transition Metal Pnictides, Springer: Berlin, **2009**, pp. 129-131. **DOI:** 10.1007/978-3-642-03420-6
32. Bhattacharyya, S.R.; Gayen, R.N.; Paul, R.; Pal, A.K.; *Thin Solid Films*, **2009**, *517*, 5530. **DOI:** 10.1016/j.tsf.2009.03.168
33. Sernelisu, B.E. Surface Modes in Physics; Wiley: Berlin, **2001**, pp. 31-32. **DOI:** 10.1002/3527603166.ch0